Physica A 686 (2026) 131352

Contents lists available at ScienceDirect

Physica A

journal homepage: www.elsevier.com/locate/physa

On the dynamics of the q-Tsallis Gauss Iterated Map

Daniel Borin [a,b,*], Matheus Rolim Sales [c,b], Edson Denis Leonel [b], Diego Fregolent Mendes de Oliveira [a]

[a] School of Electrical Engineering and Computer Science, University of North Dakota, 58202, Grand Forks, ND, USA
[b] São Paulo State University (UNESP), Institute of Geosciences and Exact Sciences, 13506-900, Rio Claro, SP, Brazil
[c] University of Essex, School of Mathematics, Statistics and Actuarial Science, Wivenhoe Park, Colchester, CO4 3SQ, United Kingdom

ARTICLE INFO

Dataset link: https://doi.org/10.5281/zenodo.17593788

ABSTRACT

We investigate the dynamical properties of a q-deformed generalization of the Gaussian iterated map, referred to as the q-Tsallis Gaussian Iterated Map, obtained by replacing the standard exponential with the Tsallis q-exponential function. Through bifurcation diagrams, Lyapunov exponent analysis, and isoperiodic diagrams, we characterize the transitions between periodic and chaotic regimes, as well as the emergence of multistability and bubbling phenomena, reveals that the introduction of the nonextensive parameter induces significant changes in the system's dynamics.

1. Introduction

Boltzmann–Gibbs (BG) statistical mechanics is one of the most fundamental frameworks in theoretical physics. Originally developed to provide an analytical description of thermodynamical quantities at thermal equilibrium, it has since been applied to a wide range of other physical systems [1–3]. The core of this theory is the Boltzmann–Gibbs entropy [4,5], defined as

$$S_{BG} = -k \sum_{i=1}^{W} p_i \ln p_i, \tag{1}$$

where k is a positive constant (typically chosen as $k = k_B$, the Boltzmann constant, or simply $k = 1$ in information theory), W is the total number of accessible micro-states, and $\{p_i\}$ are the probabilities associated with each state, satisfying $\sum_{i=1}^{W} p_i = 1$.

Despite its success, BG statistical mechanics does not adequately capture the behavior of many complex systems. These include, for example, turbulent flows [6–8], quantum entanglement [9,10], trapped ion subjected to radiofrequency heating [11], cosmic rays [12,13], high-energy particle collisions [14–18], financial markets [19–22], biological motion [23–26], and systems exhibiting classical [27–33] or quantum [34,35] chaos. In such systems, standard BG entropy often does not provide an accurate or complete description, leading to the development of more general approaches.

In response to this limitation, nonextensive statistical mechanics was proposed by Constantino Tsallis [36–41] as a generalization of BG statistical mechanics. Inspired by multifractal systems [42–44], Tsallis introduced a generalized entropy formula, known as the Tsallis entropy:

$$S_q = k \frac{1 - \sum_{i=1}^{W} p_i^q}{q - 1}, \tag{2}$$

* Corresponding author at: School of Electrical Engineering and Computer Science, University of North Dakota, 58202, Grand Forks, ND, USA.
E-mail address: d.borin@hotmail.com (D. Borin).
URL: https://danielborin.github.io/ (D. Borin).

https://doi.org/10.1016/j.physa.2026.131352
Received 3 December 2025; Received in revised form 22 January 2026
Available online 4 February 2026

where the entropic index q characterizes the degree of nonextensivity of the system. In the limit $q \to 1$, the Tsallis entropy reduces to the classical BG entropy, that is, $S_1 = S_{BG}$.

The introduction of the q-parameter provides a mechanism for deforming existing mathematical structures in order to better understand and model complex dynamical behavior. In this context, dynamical systems and maps incorporating the Tsallis formalism have attracted increasing attention, particularly for their ability to capture the effects of nonextensive statistical behavior on system dynamics. These q-deformed systems allow us to explore how dynamical properties evolve as the system deviates from the standard case, while recovering the original system in the limit $q \to 1$. In particular, modifying dynamical maps using the q-exponential or related functions allows for a detailed examination of how complexity emerges and changes with varying q, allows the study of phenomena such as bifurcations, chaos, and ergodicity from a nonextensive perspective. Beyond their theoretical importance, these deformations might also have practical application. For example, in encryption algorithms, the complexity added by nonextensive dynamics may help create more secure protocols [45–48].

In this paper, we examine the dynamics of the Gaussian map when the traditional exponential function is replaced by the Tsallis q-exponential. Our objective is to investigate how varying the level of nonextensivity influences the system's behavior, and to characterize the resulting changes in its dynamical properties. In Section 2, we introduce the q-Tsallis Gaussian iterated map and analyze its mathematical properties and behavior . Section 3 presents our results, where we explore bifurcation diagrams, Lyapunov exponents, and isoperiodic structures to characterize the influence of the q-parameter on the system's transitions between periodic and chaotic regimes, as well as the emergence of multistability and bubbling phenomena. Finally, Section 4 summarizes our findings.

2. q-Tsallis Gauss iterated map

More than 40 different entropic functionals have been proposed in the literature [39], reflecting the need to describe systems beyond the traditional framework of Boltzmann–Gibbs statistical mechanics. Among these generalizations, the Tsallis entropy has emerged as one of the most widely used. The formalism derived from Tsallis entropy is commonly known as *nonextensive statistical mechanics*. The term "nonextensive" refers to the fact that it is particularly suitable for systems with long-range interactions, where the total internal energy no longer scales linearly with system size, resulting in a breakdown of extensivity [49].

To express Tsallis entropy [Eq. (2)] in a form analogous to the classical Boltzmann entropy [Eq. (1)], one defines the q-logarithmic function as:

$$\ln_q z = \begin{cases} \dfrac{z^{1-q} - 1}{1 - q} & \text{if } q \neq 1, \\ \ln z & \text{if } q = 1, \end{cases} \tag{3}$$

for $z > 0$. Using this function, Tsallis entropy [Eq. (2)] can be rewritten as:

$$S_q = -k \sum_{i=1}^{W} p_i^q \ln_q p_i, \tag{4}$$

where k is a positive constant, p_i represents the probability of the ith microstate, W is the number of accessible microstates, and q is the entropic index characterizing the degree of nonextensivity.

The inverse of the q-logarithm is the *q-exponential function*, defined as:

$$\exp_q(z) = \begin{cases} [1 + (1 - q)z]_+^{1/(1-q)}, & \text{if } q \neq 1 \\ \exp(z), & \text{if } q = 1 \end{cases} \tag{5}$$

where $[\cdot]_+ = \max(\cdot, 0)$, ensures the function remains real-valued. This formalism leads naturally to the definition of the q-Gaussian function:

$$\exp_q(-\alpha z^2) = \begin{cases} \left[1 - (1 - q)\alpha z^2\right]_+^{1/(1-q)}, & \text{if } q \neq 1 \\ \exp(-\alpha z^2), & \text{if } q = 1 \end{cases} \tag{6}$$

where $\alpha > 0$ is a scaling parameter. The q-Gaussian reduces to the standard Gaussian distribution in the limit $q \to 1$.

A well-known dynamical system based on the Gaussian function is the *Gaussian iterated map* (also known as the Gaussian or mouse map) [50–53], defined as:

$$x_{n+1} = \exp(-a x_n^2) + b, \tag{7}$$

where x_n is the dynamical variable at iteration n, $a > 0$ and $b \in \mathbb{R}$ are control parameters. This map has been used for applications such as pseudo-random number generation and image processing [54,55].

In this work, we introduce a generalization of the Gaussian map by replacing the standard exponential function with the q-exponential function from Tsallis statistics. We refer to this model as the *q-Tsallis Gaussian Iterated Map*, which is defined by:

$$x_{n+1} = \exp_q(-\alpha x_n^2) + \beta, \tag{8}$$

where $\alpha > 0$, $\beta \in \mathbb{R}$, and $q \in \mathbb{R}$ are parameters controlling the map dynamics. It is important to note that the q-exponential function is employed here purely as a nonlinear functional form defining a deterministic iterated map, and none of the parameters

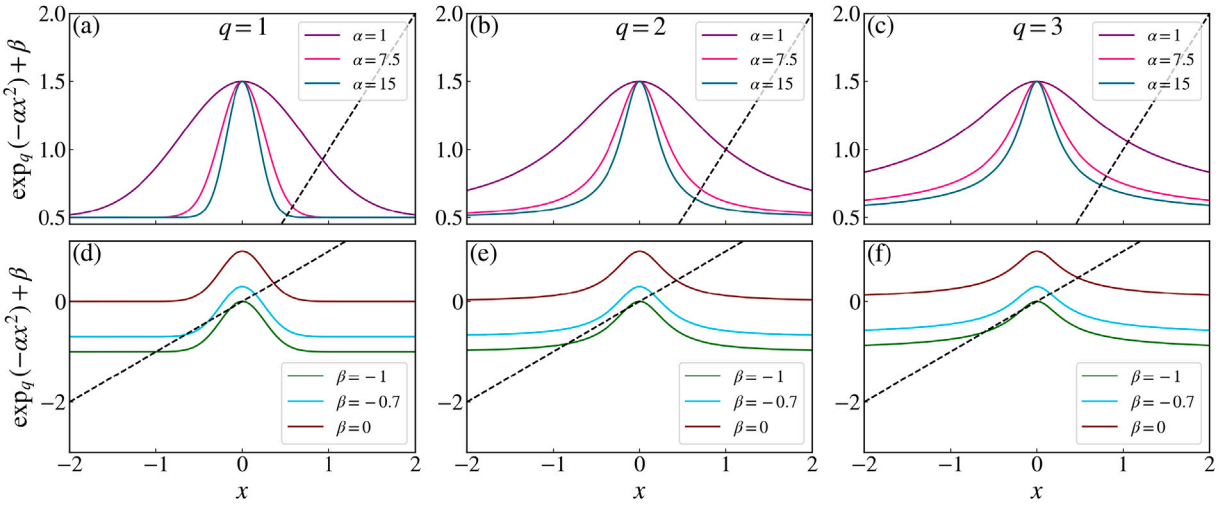

Fig. 1. Plots of the q-Tsallis Gaussian iterated function, $F(x) = \exp_q(-\alpha x_n^2) + \beta$, for three values of the entropic index: $q = 1$ (left column), $q = 2$ (middle column), and $q = 3$ (right column). (a)–(c) illustrate the function for $\alpha = 1$, 7.5, and 15, respectively, with β fixed at 0.5. In contrast, in panels (d)–(f), α is fixed at 7.5, and the function is shown for $\beta = -1$, -0.7, and 0, respectively. The black dashed line represents the identity $F(x) = x$; its intersections with the function correspond to the fixed points of the system.

introduced in Eq. (8) are assigned a probabilistic or thermodynamic interpretation. In the limit $q \to 1$, this map reduces to the classical Gaussian map [Eq. (7)], making it a natural extension within the nonextensive framework. In the context of the iterated Gauss map, we restrict the domain of the nonextensive parameter to $q > 1$ to ensure that the q-exponential function remains well-defined and avoids divergence in the calculation of the Lyapunov exponent. A comprehensive justification for this choice is provided in Appendix.

Fig. 1 presents the q-Tsallis Gaussian iterated function for various parameter sets (α, β) and for selected values of the entropic index $q = 1, 2, 3$, corresponding to the left, center, and right columns, respectively. A clear transition in the behavior of the map is observed as q varies. For $q = 1$ (Figs. 1(b) and 1(e)), the standard Gaussian form is recovered. In contrast, for $q = 2$ (Figs. 1(c) and 1(f)), the function displays heavy tails, with a slower decay compared to the standard Gaussian. For $q = 3$, as seen in Figs. 1(d) and 1(g), the function continues to exhibit even heavier tails, further deviating from the classical Gaussian form.

To better illustrate the role of the parameters in shaping the function, Figs. 1(a)–1(c) show the map with fixed $\beta = 0.5$ and varying α. The function is symmetric about $x = 0$ and achieves its maximum value, $\beta+1$, at this point. As $|x| \to \infty$, the function asymptotically approaches the minimum value β. The parameter α controls the width of the function; increasing α leads to a narrower and more sharply peaked function. Figs. 1(d)–(f) illustrate the influence of β, keeping $\alpha = 7.5$ fixed. As β increases, the function shifts upward, changing the maximum and minimum values without affecting the shape or width. This vertical displacement reveals an important feature: for sufficiently negative values of β, the function intersects the identity line $F(x) = x$ (shown in dashed black) at three points, indicating the presence of three fixed points. Therefore, the parameter β controls the number of fixed points as well as their stability.

In the next section, we will present the results of this work, including a study for which values of the parameter there are three fixed points and show how some dynamical properties are changed as we vary the degree of nonextensitivy of the system.

3. Results

In this section, we present the results of our analysis, examining how the dynamical properties of the system are influenced by the variation of the nonextensivity parameter q.

To show some of the behavior of the iterates of the Gaussian map, we plot in Fig. 2, some bifurcation diagrams for the values of the entropic index: $q = 1$ (left column), $q = 2$ (middle column), and $q = 3$ (right column). To compute these bifurcation diagrams, we iterated the q-Tsallis Gaussian map over a dense range of β values, for fixed values of α and q, and recorded the asymptotic behavior of the system after discarding transient dynamics. Specifically, in Fig. 2 for each $\beta \in [-1, 1]$, we performed 3000 iterations starting from two initial condition, $x_0 = 0$ for black and $x_0 = 10$ for red, discarded the first 2000 iterations to eliminate transients, and plotted the remaining values of the orbit as a function of β to reveal the bifurcation structure.

To better understand the system's dynamics, the analysis is conducted for two cases: $\alpha = 4.9$ (top row) and $\alpha = 7.5$ (bottom row) in Fig. 2. In the standard case, with $q = 1$, the bifurcation diagram exhibits the well-known period-doubling route to chaos: transitioning from period-one to period-two, then to period-four, and continuing through successive bifurcations that lead to chaos. However, instead of remaining in the chaotic behavior, the system reverses via a period-halving route, eventually returning to period-one. This behavior is observed for other values of q as well, where the sequence again reverses via a period-halving route, ultimately returning to period-one. This reversal, a less common route in discrete dynamical systems, can be described as *period-bubbling*.

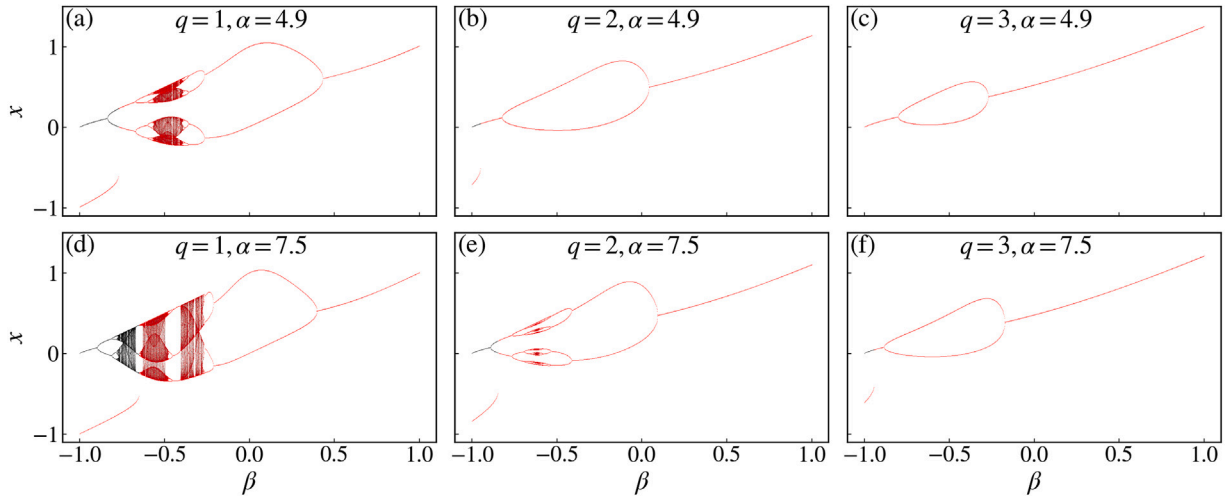

Fig. 2. Bifurcation diagrams as a function of β, for two values of α: $\alpha = 4.9$ (top row) and $\alpha = 7.5$ (bottom row), with orbits generated from initial conditions (plotted in black) and $x_0 = 10$ (plotted in red). The diagrams are shown for nonextensivity parameters $q = 1$ (left column), $q = 2$ (middle column), and $q = 3$ (right column).

Bier and Bountis [56] demonstrated that in nonlinear maps with multiple varying parameters, the typical period-doubling route to chaos may be interrupted by a period-halving transition. This dynamic leads to the formation of closed-loop structures in the bifurcation diagram (resembling bubbles) a phenomenon known as *bubbling*. Bubbling stabilizes the system temporarily around a periodic or equilibrium point; however, structural deformations in these regions can amplify fluctuations, leading to transient chaotic oscillations within the bubble. The occurrence and nature of bubbling depend exclusively on the system parameters. Bubbles are typically classified into three types based on their dynamical characteristics: (i) primary, (ii) secondary, and (iii) chaotic. These structures have been observed in several biological and dynamical systems [57–60].

As shown in Fig. 2, the bubbling phenomenon is evident. Specifically, Figs. 2(b),(c) and (f) show primary bubbling, while Fig. 2(e) illustrates secondary bubbling. Figs. 2(a) and (d) depict chaotic bubbling. As the parameter q increases, the system tends toward a more homogeneous dynamic, and a transformation in the bubble structure occurs, with a transition between different bubble types: from chaotic bubbling to secondary bubbling, and finally to primary periodic structures. These observations show that the nonextensive parameter q can suppress the bubbling phenomenon and may therefore act as an effective control mechanism for the system's dynamics . Similar results have been found using a different but similar modification in the Gaussian map [61].

It is also possible to explore how the bifurcation diagram evolves as a function of the nonextensivity parameter q. Figs. 3(a)–(c) present bifurcation diagrams of the iterated q-Tsallis Gaussian map over the interval $q \in [1, 3]$, for fixed values of $\alpha = 20$ and $\beta = -0.6, -0.4$, and -0.3, respectively. A total of 3000 iterations were performed, where the first 2000 iterations were discarded to remove transient effects, and the remaining iterations were used to construct the bifurcation plots. To further characterize this transition, the Lyapunov exponent is computed as a diagnostic tool to identify regions of chaos and periodicity.

The Lyapunov exponent provides a quantitative measure of the average exponential rate at which nearby trajectories in the system diverge or converge. It allows for a qualitative classification of the system's dynamics: a positive Lyapunov exponent indicates sensitive dependence on initial conditions and, consequently, chaotic behavior; a negative value corresponds to periodic or stable dynamics; and a zero Lyapunov exponent may signal marginal stability or quasiperiodicity [62]. In standard one-dimensional systems, the Lyapunov exponent is typically computed using the first derivative of the map. Accordingly, the Lyapunov exponent λ is given by [63]:

$$\lambda = \lim_{T\to\infty} \frac{1}{T} \sum_{n=0}^{T-1} \ln |M'(x)|, \tag{9}$$

where $M'(x)$ denotes the derivative of the map with respect to x.

In our case, the map is a q-Tsallis Gauss Iterated Map, defined by the replacement of the exponential function with the q-exponential. Accordingly, the derivative of the map is given by:

$$M'(x) = -2\alpha x[\exp_q(-\alpha x_n^2)]^q. \tag{10}$$

Figs. 3(d)–(f) show the Lyapunov exponents corresponding to each initial condition of the bifurcation diagrams in Figs. 2(a)–(c), respectively. As in the previous analysis, 3000 iterations were performed with the first 2000 discarded as transients, using $x_0 = 0$ (black) and $x_0 = 10$ (red). The dynamical regime is characterized by the sign of the Lyapunov exponent: negative values indicate periodic behavior, while positive values denote chaos.

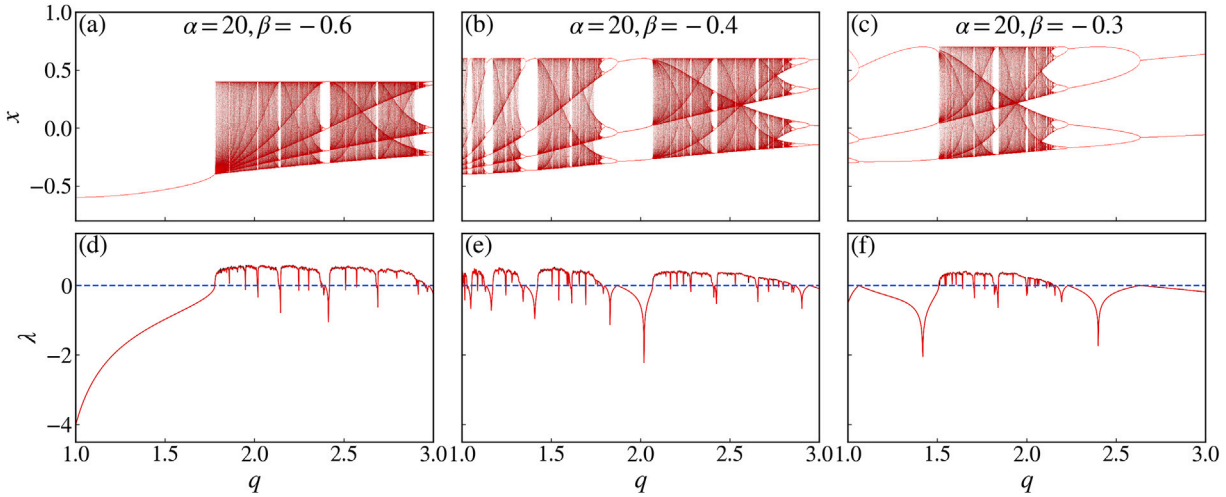

Fig. 3. Bifurcation diagrams (top row) and corresponding Lyapunov exponents (bottom row) as a function of the nonextensivity parameter q, for $\alpha = 20$ and $\beta = -0.6$ (left column), $\beta = -0.4$ (middle column), and $\beta = -0.3$ (right column).

In Section 2, it was shown that for sufficiently negative values of β, the q-Tsallis Iterated Map exhibits three fixed points. The number and stability of these fixed points, however, vary with β. Fig. 4 presents the bifurcation diagram (black points) as a function of β, obtained from 100 different initial conditions, together with the fixed points (blue, red, and green curves) for different values of q. For example, when $q = 1$ and $\beta = -1.0$, there are three fixed points: two stable (blue and green) and one unstable (red). As β increases, the fixed point shown in green loses stability through a period-doubling bifurcation. With further increases in β, successive period-doubling bifurcations occur, eventually giving rise to chaotic dynamics. Around $\beta \approx -0.9$, a chaotic attractor coexists with three fixed points: one stable (blue) and two unstable (red and green). As β continues to increase, the chaotic attractor expands and eventually collides with the red unstable fixed point, leading to its destruction in a boundary crisis [64,65]. After the destruction of the chaotic attractor, only two unstable and one stable fixed point remain. For even larger values of β, the blue (stable) and red (unstable) fixed points approach each other and eventually annihilate in a saddle–node bifurcation.

The dynamics of the fixed points do not qualitatively change with the parameter q. As q increases, the saddle–node bifurcation still occurs but for smaller values of β. However, the occurrence of the boundary crisis does depend on q. For sufficiently large q, the chaotic attractor no longer collides with the unstable fixed point and therefore never disappears [Figs. 4(e) and 4(f)].

To further explore the relationship between the coexistence of attractors and the existence of multiple fixed points, Fig. 5 presents the parametric region in which the q-Tsallis Iterated Map possesses three fixed points. The fixed points of the q-generalized Gauss map were identified by numerically solving the fixed point equation:

$$x = \exp_q(-\alpha x^2) + \beta, \tag{11}$$

which correspond to the intersections between the identity line $y = x$ and the q-Tsallis iterated Gauss map. The procedure used to find the root of Eq. (11) was the *bisection method*. Specifically, the roots of the equation were found by evaluating the residual function

$$f(x) = x - \exp_q(-\alpha x^2) - \beta, \tag{12}$$

over the interval $[-2, 2]$, divided into 10^3 subintervals. For each pair of adjacent points, a sign change in $f(x)$ was interpreted as an indication of a root in the subinterval. Subsequently, the bisection method was applied to refine the location of the root, using a tolerance of 10^{-8}. To avoid numerical duplication, each detected root was compared with previously identified roots, and only those differing by more than the tolerance were retained. The analysis was conducted for different values of the nonextensivity parameter: $q = 1$ [Fig. 5(a)], $q = 2$ [Fig. 5(b)], and $q = 3$ [Fig. 5(c)]. It can be observed that as q increases, the region in which the map has three fixed points becomes smaller.

To investigate the relationship between this region and the coexistence of attractors, the presence of multistability in the q-Tsallis Iterated Gauss map was examined in Fig. 5(d)–(f). The analysis was performed by iterating the map from a collection of distinct initial conditions and comparing the resulting asymptotic behaviors. For a given set of parameters (α, β, q), the map was iterated 1.1×10^4 times from multiple initial conditions $x_0 \in [-10, 10]$. As the focus is on the long-term dynamics, a transient of 10^3 iterations was discarded. To determine whether an orbit settled into a periodic attractor, the current state was compared to previously visited states after the transient. If a state repeated within a numerical tolerance 10^{-8}, the trajectory was classified as periodic. Otherwise, the orbit was considered aperiodic or chaotic. The coexistence of attractors was identified by comparing the asymptotic behaviors obtained from different initial conditions, using the same numerical tolerance of 10^{-8} as the proximity criterion. The analysis, similar

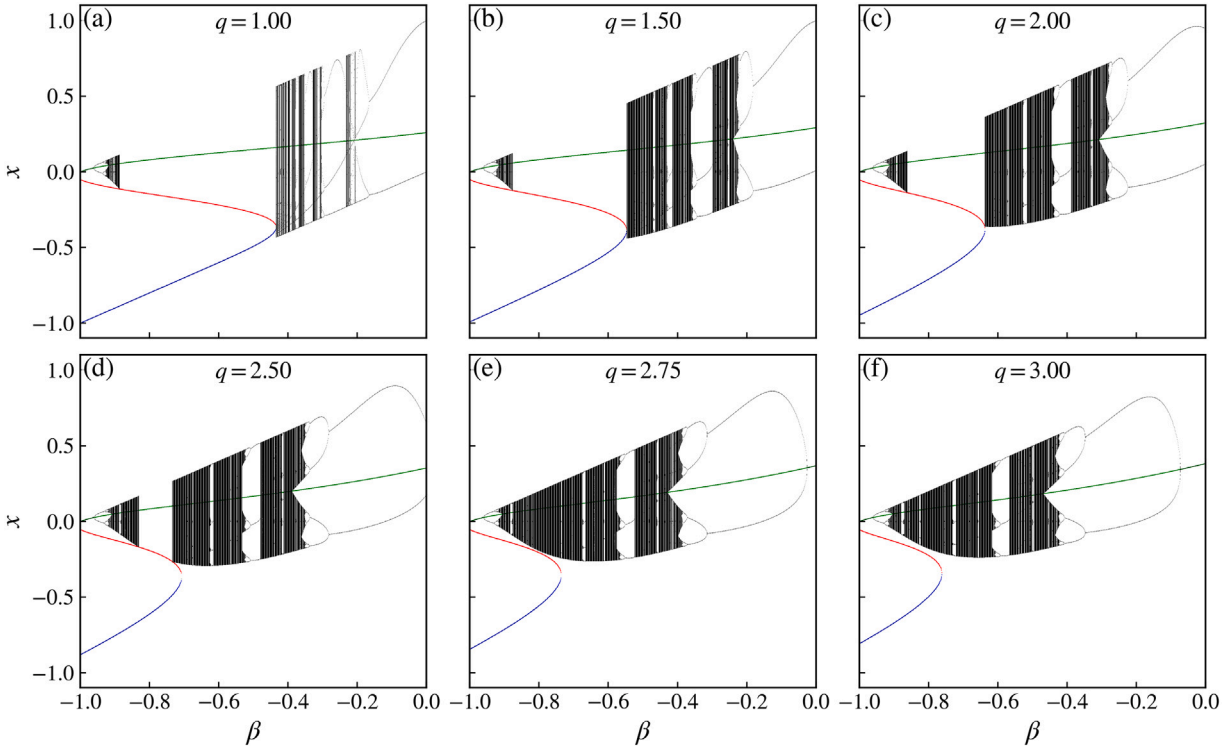

Fig. 4. Bifurcation diagram (black points) together with the fixed points (blue, red, and green curves) as a function of β for $\alpha = 20.0$ with different values of q. The bifurcation diagram was generated using 100 initial conditions uniformly distributed within the interval $x \in [-1, 1]$. The collision between the unstable fixed point (red curve) and the chaotic attractor is evident in panels (a)–(d).

to Fig. 5(a)–(c) was conducted for different values of the nonextensivity parameter: $q = 1$ (Fig. 5(d)), $q = 2$ [Fig. 5(e)], and $q = 3$ (Fig. 5(f)).

It is interesting to note that the region of the parameter space in Fig. 5(c)–(d), where co-existing attractors exist, is a subset of the region shown in Fig. 5(a)–(c), which confirms our earlier conclusion that the emergence of co-existing attractors at a particular set of parameters can be understood as a consequence of presence of three fixed points. However, the converse is not always true as it is clear from Fig. 5 that there is a part of parameter space, where three fixed points exist but co-existing attractors are not present. In Fig. 5(a)–(c), we have identified different regions of parameter space (α, β) where the dynamics of q-Gaussian map is chaotic or regular (purple shades correspond to chaotic, otherwise correspond to periodic attractors) for different values of the nonextensivity parameter q. These regions corresponding to values of Lyapunov exponent greater than 0, which was computed considering the same time of interaction and transient used to generate the region of multistability. The points where the color purple and black coexist there are the region regular and chaotic motions co-exist along with the region of co-existing attractors.

Analyzing only regions where the Lyapunov exponent is positive offers a limited perspective of the system's dynamics, as it overlooks the presence of periodic windows that occur in regions with negative Lyapunov exponents. In the parameter space shown in Fig. 6(a)–(c), we observe a complex interplay between chaotic (orange to white) and regular (blue to black) regimes for different values of the nonextensivity parameter q. As one or both control parameters are varied, transitions between chaotic and periodic behavior are observed, with regions of chaos giving way to periodic dynamics and vice versa, leading to the formation of narrow periodic windows embedded within the chaotic domain.

To better characterize the structure of these periodic orbits and the transitions between them, Fig. 7(a)–(c) presents isoperiodic diagrams for various values of q. These diagrams were generated by setting the initial condition $x_0 = 0$ and computing the period of orbits on a grid in the (α, β) parameter-space. The period is defined as the number of iterations required for the orbit to revisit a previous value in its time series, after discarding a transient of 5×10^4 iterations. If no periodicity is detected within 6×10^4 iterations, the orbit is classified as chaotic and represented in white. Different colors are associated with different periods of the trajectories and values besides the numeric legend (i.e. bigger than 15) are in gray color. The diagrams reveal that stable (periodic) behavior occupies a significant portion of the parameter space. Periodic regions coexist with period-doubling cascades—for example, period-3 and period-6 regions are found adjacent to each other, as are period-6 and period-12 regions.

Fig. 7(d)–(f) provide magnifications of regions where chaotic and periodic behaviors coexist. For $q = 1$, the chaotic domain shrinks and periodic regions become more prominent. In contrast, as q increases (e.g., $q = 2$ and $q = 3$), this behavior is reversed: the chaotic regions grow more prominent while periodic windows narrow. This illustrates how the degree of nonextensivity significantly influences the balance between order and chaos in the system.

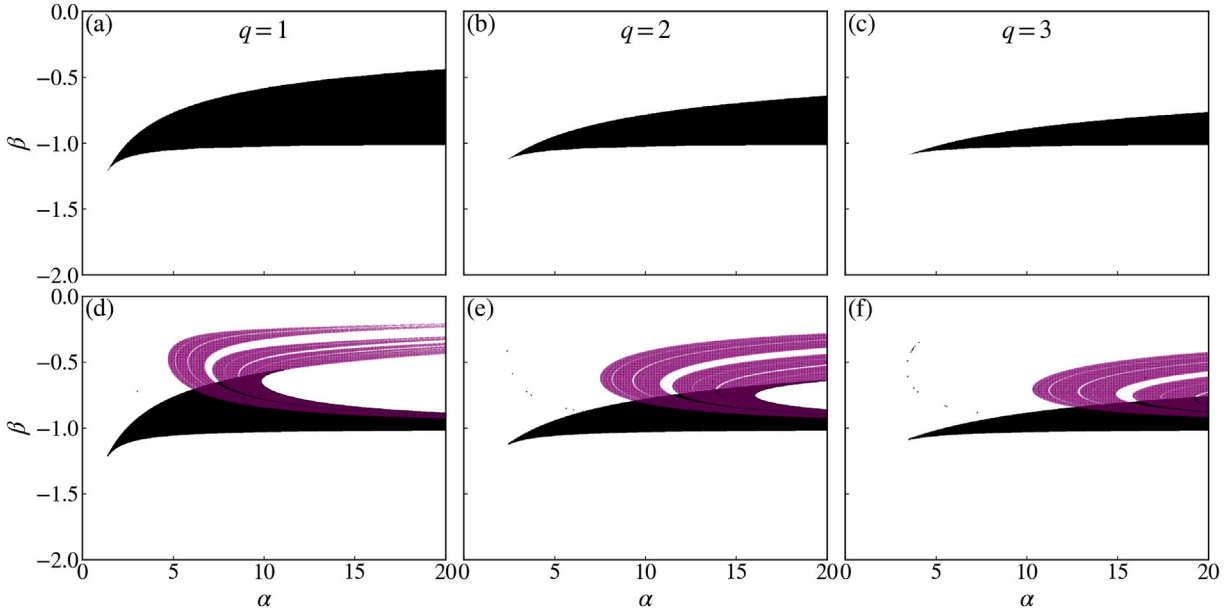

Fig. 5. Parameter space (α, β) showing the regions in black where the Gaussian map possesses three fixed points (top row), and the regions where it exhibits co-existing attractors and chaotic motion, indicated by black and purple colors, respectively (bottom row). The diagrams correspond to nonextensivity parameters $q = 1$ (left column), $q = 2$ (middle column), and $q = 3$ (right column).

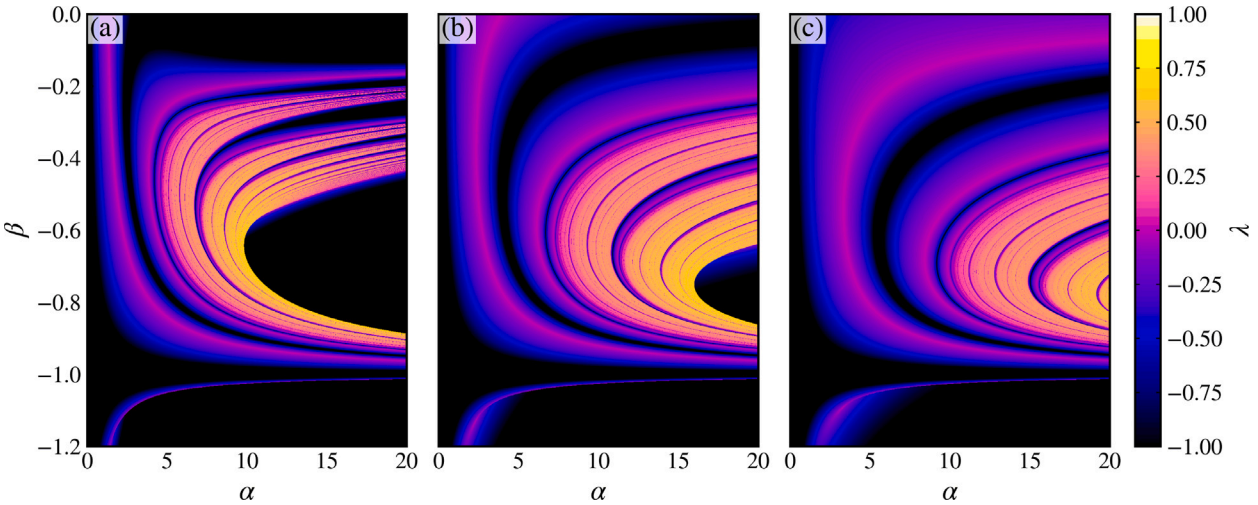

Fig. 6. The Lyapunov exponent λ in parameter space $\alpha \times \beta$ with (a) $q = 1$, (b) $q = 2$, and (c) $q = 3$. The colors from blue to black (pink to white) correspond to periodic (chaotic) dynamics, whereas the purple color (vanishing λ) marks the bifurcation points.

4. Conclusion

We have proposed the q-Tsallis Gaussian iterated map, a generalization of the classical Gaussian map using Tsallis statistics, that incorporates the nonextensive parameter q through the q-exponential function. Our investigation demonstrated how the degree of nonextensivity significantly influences the system's dynamical behavior, including the number of fixed points, the emergence and structure of bifurcations, the presence of coexisting attractors, and the transition between periodic and chaotic regimes.

We have demonstrated via bifurcation diagrams as a function of β that the system undergoes period-doubling routes to chaos, interrupted by period-halving reversals, arising the phenomenon termed "bubbling". The nonextensive parameter q can suppress this bubbling, acting as an effective control mechanism. By analyzing bifurcation diagrams and Lyapunov exponents as q varies, we have shown that the system initially exhibits chaotic dynamics, which are subsequently followed by a period-halving route.

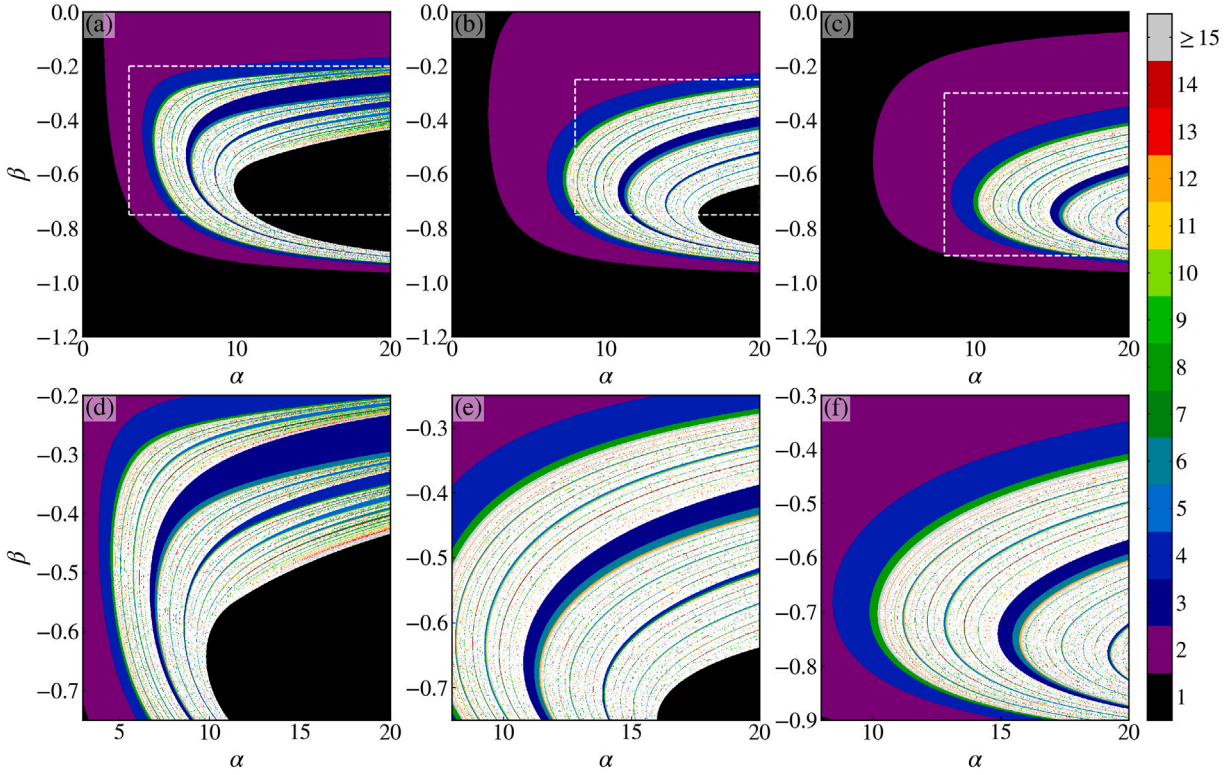

Fig. 7. The isoperiodic diagram in parameter space $\alpha \times \beta$ with (a) $q = 1$, (b) $q = 2$, and (c) $q = 3$. The colored regions correspond to different periods within the periodic domains, while white region indicates to chaotic dynamics. (d), (e) and (f) are magnifications of the regions bounded by the white dashed rectangles in (a), (b) and (c), respectively.

For certain parameter ranges, the map exhibits three fixed points. These fixed points often coexist with a chaotic attractor, leading to the presence of multiple coexisting attractors. This coexistence persists until the chaotic attractor expands and collides with an unstable fixed point, resulting in its destruction in a boundary crisis. The parameter q plays a key role in anticipating or delaying this boundary crisis, effectively acting as a control mechanism. Additionally, the parametric analysis highlighted how regions of multistability and chaos evolve with changes in q, where the regions of multistability shrink and chaotic region becomes more dense as q increases.

Lyapunov exponent calculations confirm the presence of chaotic and periodic windows for several values of q. Isoperiodic diagrams further reveal intricate structures of periodic domains embedded within chaotic regions, underlining the role of nonextensivity in shaping the global dynamics of the system.

Finally, it is instructive to distinguish between topological and metrical modifications induced by the nonextensive parameter q when compared to the standard Gaussian map ($q = 1$). From a topological perspective, the global organization of the dynamics is preserved: the system continues to exhibit fixed points, period-doubling cascades, bubbling phenomena, multistability, and boundary crises, indicating that the qualitative structure of the phase space remains unchanged. In contrast, the introduction of q produces significant metrical effects, including shifts in bifurcation thresholds, deformation of stability boundaries, changes in the extent of multistable regions, suppression or enhancement of bubbling structures, and variations in the size and density of chaotic and periodic domains. Thus, the q-deformation acts primarily as a quantitative modulator of the dynamics rather than inducing a qualitative topological reorganization.

CRediT authorship contribution statement

Daniel Borin: Writing – review & editing, Writing – original draft, Visualization, Validation, Software, Project administration, Methodology, Investigation, Formal analysis, Data curation, Conceptualization. **Matheus Rolim Sales:** Writing – review & editing, Validation, Software, Methodology, Investigation, Formal analysis, Data curation. **Edson Denis Leonel:** Writing – review & editing, Validation, Resources, Funding acquisition, Formal analysis. **Diego Fregolent Mendes de Oliveira:** Writing – review & editing, Validation, Supervision, Resources, Methodology, Formal analysis.

Declaration of competing interest

The authors declare that they have no known competing financial interests or personal relationships that could have appeared to influence the work reported in this paper.

Acknowledgments

This study was financed, in part, by the São Paulo Research Foundation (FAPESP), Brazil. Process Numbers #2024/06749-8, #2024/09208-8, #2023/08698-9, #2022/03612-6, #2019/14038-6, and #2021/09519-5. E. D. Leonel also acknowledges support from Brazilian agency CNPq (No. 301318/2019-0, 304398/2023-3)

Appendix. Justification for the choice $q > 1$

In this appendix, we provide a detailed explanation for the choice of the domain $q > 1$ in the generalization of the iterated Gauss map using the q-Tsallis exponential function. The q-exponential is defined as:

$$\exp_q(z) = \begin{cases} [1 + (1-q)z]_+^{1/(1-q)}, & \text{if } q \neq 1 \\ \exp(z), & \text{if } q = 1 \end{cases} \tag{A.1}$$

where $[\cdot]_+ = \max(\cdot, 0)$, ensuring that the function remains real-valued. The standard exponential function is recovered in the limit $q \to 1$. This expression is positive only when the base $1 + (1-q)z$ is non-negative.

In the context of the iterated Gauss map, we frequently use $\exp_q(-\alpha x^2)$, where $x \in \mathbb{R}$ and $\alpha > 0$. Since $-\alpha x^2 \leq 0$ for all real x, we examine the conditions under which the function remains positive.

For $q < 1$, the term $(1-q)$ becomes positive, and the base $1 + (1-q)(-\alpha x^2)$ remains non-negative only if:

$$x^2 < \frac{1}{(1-q)\alpha}. \tag{A.2}$$

Thus, for values of $|x| \geq \frac{1}{\sqrt{(1-q)\alpha}}$, the base becomes negative, which would cause the function to assume a zero value. This is problematic for our calculations, particularly when computing the Lyapunov exponent, as we take the logarithm of the derivative. The logarithmic function $\ln|-2\alpha x[\exp_q(-\alpha x^2)]^q|$ becomes undefined when the argument inside the logarithm is zero. Therefore, if $\exp_q(-\alpha x^2) = 0$, the logarithm diverges, leading to a non-physical, infinite result.

In contrast, for $q > 1$, the term $(1-q)$ is negative, and the base $1 + (1-q)(-\alpha x^2)$ remains positive for all real x, ensuring the function stays well-defined and non-zero across the entire real line.

Thus, to avoid undefined behavior in the calculation of the Lyapunov exponent and ensure the function remains well-defined for all $x \in \mathbb{R}$, we restrict the domain of the nonextensive parameter to $q > 1$.

Data availability

The source code to reproduce the results of this paper is available at Zenodo: https://doi.org/10.5281/zenodo.17593788.

References

[1] R. Pathria, P.D. Beale, Statistical Mechanics, Elsevier, NewYork, 2011.
[2] A. Spanos, Statistical Foundations of Econometric Modelling, Cambridge University Press, 1986.
[3] F. Reif, Fundamentals of Statistical and Thermal Physics, Waveland Press, 2009.
[4] J.W. Gibbs, Elementary Principles in Statistical Mechanics: Developed with Especial Reference to the Rational Foundations of Thermodynamics, C. Scribner's sons, 1902.
[5] L. Boltzmann, Studien über das Gleichgewicht der lebendigen Kraft zwischen bewegten materiellen Punkten: vorgelegt in der Sitzung am 8. October 1868, k. und k. Hof- und Staatsdr., 1868.
[6] C. Beck, Dynamical foundations of nonextensive statistical mechanics, Phys. Rev. Lett. 87 (2001) 180601, http://dx.doi.org/10.1103/PhysRevLett.87.180601, URL https://link.aps.org/doi/10.1103/PhysRevLett.87.180601.
[7] C. Beck, G.S. Lewis, H.L. Swinney, Measuring nonextensitivity parameters in a turbulent Couette–Taylor flow, Phys. Rev. E 63 (2001) 035303, http://dx.doi.org/10.1103/PhysRevE.63.035303, URL https://link.aps.org/doi/10.1103/PhysRevE.63.035303.
[8] T. Arimitsu, N. Arimitsu, PDF of velocity fluctuation in turbulence by a statistics based on generalized entropy, Phys. A 305 (1) (2002) 218–226, http://dx.doi.org/10.1016/S0378-4371(01)00665-3, Non Extensive Thermodynamics and Physical applications, URL https://www.sciencedirect.com/science/article/pii/S0378437101006653.
[9] C. Tsallis, S. Lloyd, M. Baranger, Peres criterion for separability through nonextensive entropy, Phys. Rev. A 63 (2001) 042104, http://dx.doi.org/10.1103/PhysRevA.63.042104, URL https://link.aps.org/doi/10.1103/PhysRevA.63.042104.
[10] S. Abe, A. Rajagopal, Nonadditive conditional entropy and its significance for local realism, Phys. A 289 (1) (2001) 157–164, http://dx.doi.org/10.1016/S0378-4371(00)00476-3, URL https://www.sciencedirect.com/science/article/pii/S0378437100004763.
[11] R. Wild, M. Nötzold, M. Simpson, T.D. Tran, R. Wester, Tunnelling measured in a very slow ion–molecule reaction, Nature 615 (7952) (2023) 425–429, http://dx.doi.org/10.1038/s41586-023-05727-z.
[12] C. Beck, Generalized statistical mechanics of cosmic rays, Phys. A 331 (1) (2004) 173–181, http://dx.doi.org/10.1016/j.physa.2003.09.025, URL https://www.sciencedirect.com/science/article/pii/S0378437103008665.
[13] C. Tsallis, J.C. Anjos, E.P. Borges, Fluxes of cosmic rays: a delicately balanced stationary state, Phys. Lett. A 310 (5) (2003) 372–376, http://dx.doi.org/10.1016/S0375-9601(03)00377-3, URL https://www.sciencedirect.com/science/article/pii/S0375960103003773.

[14] L. Marques, J. Cleymans, A. Deppman, Description of high-energy pp collisions using Tsallis thermodynamics: Transverse momentum and rapidity distributions, Phys. Rev. D 91 (2015) 054025, http://dx.doi.org/10.1103/PhysRevD.91.054025, URL https://link.aps.org/doi/10.1103/PhysRevD.91.054025.

[15] L. Marques, E. Andrade-II, A. Deppman, Nonextensivity of hadronic systems, Phys. Rev. D 87 (2013) 114022, http://dx.doi.org/10.1103/PhysRevD.87.114022, URL https://link.aps.org/doi/10.1103/PhysRevD.87.114022.

[16] I. Bediaga, E. Curado, J. de Miranda, A nonextensive thermodynamical equilibrium approach in e+e- → hadrons, Phys. A 286 (1) (2000) 156–163, http://dx.doi.org/10.1016/S0378-4371(00)00368-X, URL https://www.sciencedirect.com/science/article/pii/S037843710000368X.

[17] S.D. Campos, V.A. Okorokov, C.V. Moraes, The tsallis entropy and the BKT-like phase transition in the impact parameter space for pp and $\bar{p}p$ collisions, Phys. Scr. 95 (2) (2020) 025301, http://dx.doi.org/10.1088/1402-4896/ab429e.

[18] L.Q. Rocha, E. Megías, L.A. Trevisan, K.K. Olimov, F. Liu, A. Deppman, Nonextensive statistics in high energy collisions, Physics 4 (2) (2022) 659–671, http://dx.doi.org/10.3390/physics4020044, URL https://www.mdpi.com/2624-8174/4/2/44.

[19] L. Borland, Option pricing formulas based on a non-Gaussian stock price model, Phys. Rev. Lett. 89 (2002) 098701, http://dx.doi.org/10.1103/PhysRevLett.89.098701, URL https://link.aps.org/doi/10.1103/PhysRevLett.89.098701.

[20] W.O. Sosa-Correa, A.M. Ramos, G.L. Vasconcelos, Investigation of non-Gaussian effects in the Brazilian option market, Phys. A 496 (2018) 525–539, http://dx.doi.org/10.1016/j.physa.2017.12.115, URL https://www.sciencedirect.com/science/article/pii/S037843711731364X.

[21] F. Michael, M. Johnson, Financial market dynamics, Phys. A 320 (2003) 525–534, http://dx.doi.org/10.1016/S0378-4371(02)01558-3, URL https://www.sciencedirect.com/science/article/pii/S0378437102015583.

[22] C. Anteneodo, C. Tsallis, A.S. Martinez, Risk aversion in economic transactions, Europhys. Lett. 59 (5) (2002) 635, http://dx.doi.org/10.1209/epl/i2002-00172-5.

[23] S.-Z. Lin, P.-C. Chen, L.-Y. Guan, Y. Shao, Y.-K. Hao, Q. Li, B. Li, D.A. Weitz, X.-Q. Feng, Universal statistical laws for the velocities of collective migrating cells, Adv. Biosyst. 4 (8) (2020) 2000065, http://dx.doi.org/10.1002/adbi.202000065, arXiv:https://onlinelibrary.wiley.com/doi/pdf/10.1002/adbi.202000065 URL https://onlinelibrary.wiley.com/doi/abs/10.1002/adbi.202000065.

[24] A. Upadhyaya, J.-P. Rieu, J.A. Glazier, Y. Sawada, Anomalous diffusion and non-Gaussian velocity distribution of hydra cells in cellular aggregates, Phys. A 293 (3) (2001) 549–558, http://dx.doi.org/10.1016/S0378-4371(01)00009-7, URL https://www.sciencedirect.com/science/article/pii/S0378437101000097.

[25] F. Fernández-Navarro, C. Hervás-Martínez, M. Cruz-Ramírez, P.A. Gutiérrez, A. Valero, Evolutionary q-Gaussian radial basis function neural network to determine the microbial growth/no growth interface of *Staphylococcus aureus*, Appl. Soft Comput. 11 (3) (2011) 3012–3020, http://dx.doi.org/10.1016/j.asoc.2010.11.027, URL https://www.sciencedirect.com/science/article/pii/S1568494610003042.

[26] L. Diambra, L. Cintra, Q. Chen, D. Schubert, L. da F. Costa, Cell adhesion protein decreases cell motion: Statistical characterization of locomotion activity, Phys. A 365 (2) (2006) 481–490, http://dx.doi.org/10.1016/j.physa.2005.10.006, URL https://www.sciencedirect.com/science/article/pii/S0378437105010770.

[27] G.F.J. Añaños, C. Tsallis, Ensemble averages and nonextensivity at the edge of chaos of one-dimensional maps, Phys. Rev. Lett. 93 (2004) 020601, http://dx.doi.org/10.1103/PhysRevLett.93.020601, URL https://link.aps.org/doi/10.1103/PhysRevLett.93.020601.

[28] M.L. Lyra, C. Tsallis, Nonextensivity and multifractality in low-dimensional dissipative systems, Phys. Rev. Lett. 80 (1998) 53–56, http://dx.doi.org/10.1103/PhysRevLett.80.53, URL https://link.aps.org/doi/10.1103/PhysRevLett.80.53.

[29] F.A.B.F. de Moura, U. Tirnakli, M.L. Lyra, Convergence to the critical attractor of dissipative maps: Log-periodic oscillations, fractality, and nonextensivity, Phys. Rev. E 62 (2000) 6361–6365, http://dx.doi.org/10.1103/PhysRevE.62.6361, URL https://link.aps.org/doi/10.1103/PhysRevE.62.6361.

[30] F. Baldovin, A. Robledo, Universal renormalization-group dynamics at the onset of chaos in logistic maps and nonextensive statistical mechanics, Phys. Rev. E 66 (2002) 045104, http://dx.doi.org/10.1103/PhysRevE.66.045104, URL https://link.aps.org/doi/10.1103/PhysRevE.66.045104.

[31] U. Tirnakli, E.P. Borges, The standard map: From Boltzmann-Gibbs statistics to Tsallis statistics, Sci. Rep. 6 (1) (2016) 23644, http://dx.doi.org/10.1038/srep23644, URL https://www.nature.com/articles/srep23644.

[32] K. Cetin, U. Tirnakli, B.M. Boghosian, A generalization of the standard map and its statistical characterization, Sci. Rep. 12 (1) (2022) 8575, http://dx.doi.org/10.1038/s41598-022-12213-5, URL https://www.nature.com/articles/s41598-022-12213-5.

[33] K. Cetin, U. Tirnakli, D.F. Oliveira, E.D. Leonel, Statistical mechanical characterization of billiard systems, Chaos Solitons Fractals 178 (2024) 114331.

[34] Y.S. Weinstein, S. Lloyd, C. Tsallis, Border between regular and chaotic quantum dynamics, Phys. Rev. Lett. 89 (2002) 214101, http://dx.doi.org/10.1103/PhysRevLett.89.214101, URL https://link.aps.org/doi/10.1103/PhysRevLett.89.214101.

[35] H. Santos Lima, M.M.A. Paixão, C. Tsallis, de Broglie–Bohm analysis of a nonlinear membrane: From quantum to classical chaos, Chaos: An Interdiscip. J. Nonlinear Sci. 34 (2) (2024) 023125, http://dx.doi.org/10.1063/5.0175044.

[36] C. Tsallis, Possible generalization of Boltzmann-Gibbs statistics, J. Stat. Phys. 52 (1988) 479–487.

[37] E.M.F. Curado, C. Tsallis, Generalized statistical mechanics: connection with thermodynamics, J. Phys. A: Math. Gen. 24 (2) (1991) L69, http://dx.doi.org/10.1088/0305-4470/24/2/004.

[38] C. Tsallis, R. Mendes, A. Plastino, The role of constraints within generalized nonextensive statistics, Phys. A 261 (3) (1998) 534–554, http://dx.doi.org/10.1016/S0378-4371(98)00437-3, URL https://www.sciencedirect.com/science/article/pii/S0378437198004373.

[39] C. Tsallis, Introduction to Nonextensive Statistical Mechanics: Approaching a Complex World, vol. 1, (1) Springer, 2009.

[40] C. Tsallis, Nonadditive entropy and nonextensive statistical mechanics-an overview after 20 years, Braz. J. Phys. 39 (2009) 337–356.

[41] S. Umarov, T. Constantino, Mathematical Foundations of Nonextensive Statistical Mechanics, World Scientific, 2022.

[42] H. Hentschel, I. Procaccia, The infinite number of generalized dimensions of fractals and strange attractors, Phys. D: Nonlinear Phenom. 8 (3) (1983) 435–444, http://dx.doi.org/10.1016/0167-2789(83)90235-X, URL https://www.sciencedirect.com/science/article/pii/016727898390235X.

[43] T.C. Halsey, M.H. Jensen, L.P. Kadanoff, I. Procaccia, B.I. Shraiman, Fractal measures and their singularities: The characterization of strange sets, Phys. Rev. A 33 (1986) 1141–1151, http://dx.doi.org/10.1103/PhysRevA.33.1141, URL https://link.aps.org/doi/10.1103/PhysRevA.33.1141.

[44] G. Paladin, A. Vulpiani, Anomalous scaling laws in multifractal objects, Phys. Rep. 156 (4) (1987) 147–225, http://dx.doi.org/10.1016/0370-1573(87)90110-4, URL https://www.sciencedirect.com/science/article/pii/0370157387901104.

[45] A. Al-Hyari, M. Abu-Faraj, C. Obimbo, M. Alazab, Chaotic Hénon–Logistic map integration: A powerful approach for safeguarding digital images, J. Cybersecur. Priv. 5 (1) (2025) http://dx.doi.org/10.3390/jcp5010008, URL https://www.mdpi.com/2624-800X/5/1/8.

[46] N. Singh, A. Sinha, Optical image encryption using hartley transform and logistic map, Opt. Commun. 282 (6) (2009) 1104–1109, http://dx.doi.org/10.1016/j.optcom.2008.12.001, URL https://www.sciencedirect.com/science/article/pii/S0030401808012443.

[47] M. Baptista, Cryptography with chaos, Phys. Lett. A 240 (1) (1998) 50–54, http://dx.doi.org/10.1016/S0375-9601(98)00086-3, URL https://www.sciencedirect.com/science/article/pii/S0375960198000863.

[48] S. Kumar, M. Kumar, R. Budhiraja, M. Das, S. Singh, A cryptographic model for better information security, J. Inf. Secur. Appl. 43 (2018) 123–138, http://dx.doi.org/10.1016/j.jisa.2018.10.011, URL https://www.sciencedirect.com/science/article/pii/S2214212618302825.

[49] C. Tsallis, Non-additive entropies and statistical mechanics at the edge of chaos: a bridge between natural and social sciences, Philos. Trans. R. Soc. A: Math. Phys. Eng. Sci. 381 (2256) (2023) 20220293, http://dx.doi.org/10.1098/rsta.2022.0293, arXiv:https://royalsocietypublishing.org/doi/pdf/10.1098/rsta.2022.0293 URL https://royalsocietypublishing.org/doi/abs/10.1098/rsta.2022.0293.

[50] R.C. Hilborn, Chaos and Nonlinear Dynamics: An Introduction for Scientists and Engineers, Oxford University Press, 2000.

[51] J.A. de Oliveira, H.M. de Mendonça, A.A. da Silva, E.D. Leonel, Critical slowing down at a fold and a period doubling bifurcations for a gauss map, Braz. J. Phys. 49 (2019) 923–927.
[52] J. Cánovas, M. Muñoz-Guillermo, On the dynamics of the q-deformed Gaussian map, Int. J. Bifurc. Chaos 30 (08) (2020) 2030021, http://dx.doi.org/10.1142/S0218127420300219.
[53] V. Patidar, K. Sud, A comparative study on the co-existing attractors in the Gaussian map and its q-deformed version, Commun. Nonlinear Sci. Numer. Simul. 14 (3) (2009) 827–838, http://dx.doi.org/10.1016/j.cnsns.2007.10.015, URL https://www.sciencedirect.com/science/article/pii/S1007570407003164.
[54] A. Shafique, A noise-tolerant cryptosystem based on the decomposition of bit-planes and the analysis of chaotic gauss iterated map, Neural Comput. Appl. 34 (19) (2022) 16805–16828.
[55] A. Sahay, C. Pradhan, Gauss iterated map based RGB image encryption approach, in: 2017 International Conference on Communication and Signal Processing, ICCSP, IEEE, 2017, pp. 0015–0018.
[56] M. Bier, T.C. Bountis, Remerging feigenbaum trees in dynamical systems, Phys. Lett. A 104 (5) (1984) 239–244, http://dx.doi.org/10.1016/0375-9601(84)90059-8, URL https://www.sciencedirect.com/science/article/pii/0375960184900598.
[57] E. Liz, A. Ruiz-Herrera, The hydra effect, bubbles, and chaos in a simple discrete population model with constant effort harvesting, J. Math. Biol. 65 (2012) 997–1016, http://dx.doi.org/10.1007/s00285-011-0489-2.
[58] E.F. Zipkin, C.E. Kraft, E.G. Cooch, P.J. Sullivan, When can efforts to control nuisance and invasive species backfire? Ecol. Appl. 19 (6) (2009) 1585–1595, http://dx.doi.org/10.1890/08-1467.1, arXiv:https://esajournals.onlinelibrary.wiley.com/doi/pdf/10.1890/08-1467.1 URL https://esajournals.onlinelibrary.wiley.com/doi/abs/10.1890/08-1467.1.
[59] Aishwaraya, D. Gupta, V.V.M.S. Chandramouli, Dynamics of q deformed ricker map, J. Difference Equ. Appl. 28 (11–12) (2022) 1423–1448, http://dx.doi.org/10.1080/10236198.2022.2142468.
[60] E. Liz, Complex dynamics of survival and extinction in simple population models with harvesting, Theor. Ecol. 3 (2010) 209–221, http://dx.doi.org/10.1007/s12080-009-0064-2.
[61] P. Deb, G.C. Layek, Controlling the period-bubbling route to chaos, Int. J. Bifurc. Chaos 34 (10) (2024) 2450123, http://dx.doi.org/10.1142/S0218127424501232.
[62] A. Wolf, J.B. Swift, H.L. Swinney, J.A. Vastano, Determining Lyapunov exponents from a time series, Phys. D: Nonlinear Phenom. 16 (3) (1985) 285–317, http://dx.doi.org/10.1016/0167-2789(85)90011-9, URL https://www.sciencedirect.com/science/article/pii/0167278985900119.
[63] E. Ott, Chaos in Dynamical Systems, Cambridge University Press, 2002.
[64] C. Grebogi, E. Ott, J.A. Yorke, Chaotic attractors in crisis, Phys. Rev. Lett. 48 (1982) 1507–1510, http://dx.doi.org/10.1103/PhysRevLett.48.1507, URL https://link.aps.org/doi/10.1103/PhysRevLett.48.1507.
[65] C. Grebogi, E. Ott, J.A. Yorke, Crises, sudden changes in chaotic attractors, and transient chaos, Phys. D: Nonlinear Phenom. 7 (1) (1983) 181–200, http://dx.doi.org/10.1016/0167-2789(83)90126-4, URL https://www.sciencedirect.com/science/article/pii/0167278983901264.